Science Translational Medicine
AAAS

Photoactivation of Endogenous Latent Transforming Growth Factor–β1 Directs Dental Stem Cell Differentiation for Regeneration

Praveen R. Arany *et al.*

Sci Transl Med **6**, 238ra69 (2014);
DOI: 10.1126/scitranslmed.3008234

Editor's Summary

Laser Light Encourages Tooth Regeneration

A small dose of light may be sufficient to promote new tooth growth, at least in animal models. Arany and colleagues shined low-power laser light on the tooth pulps of rats and saw the formation of tertiary dentin, which is a bone-like substance. Taking this as evidence of tooth regeneration, the authors investigated the mechanism by which light can cause the dental pulp to form bone. Arany *et al.* discovered that low-power laser activates latent transforming growth factor–β (TGF-β), leading to the generation of reactive oxygen species and the differentiation of dental stem cells into odontoblasts (dentin-forming bone cells). This mechanism was further confirmed in vivo by demonstrating that mice lacking TGF-β or treated with a TGF-β inhibitor were unable to respond to laser therapy. Because lasers are already used in dentistry, it is possible that such light-based treatment could be used in dental regeneration in people.

Science Translational Medicine (print ISSN 1946-6234; online ISSN 1946-6242) is published weekly, except the last week in December, by the American Association for the Advancement of Science, 1200 New York Avenue NW, Washington, DC 20005.

REGENERATIVE MEDICINE

Photoactivation of Endogenous Latent Transforming Growth Factor–β1 Directs Dental Stem Cell Differentiation for Regeneration

Praveen R. Arany,[1,2,3,4,5] Andrew Cho,[5] Tristan D. Hunt,[1] Gursimran Sidhu,[1] Kyungsup Shin,[1,3] Eason Hahm,[1] George X. Huang,[1] James Weaver,[2] Aaron Chih-Hao Chen,[6] Bonnie L. Padwa,[7] Michael R. Hamblin,[6,8,9] Mary Helen Barcellos-Hoff,[10] Ashok B. Kulkarni,[5] David J. Mooney[1,2]*

Rapid advancements in the field of stem cell biology have led to many current efforts to exploit stem cells as therapeutic agents in regenerative medicine. However, current ex vivo cell manipulations common to most regenerative approaches create a variety of technical and regulatory hurdles to their clinical translation, and even simpler approaches that use exogenous factors to differentiate tissue-resident stem cells carry significant off-target side effects. We show that non-ionizing, low-power laser (LPL) treatment can instead be used as a minimally invasive tool to activate an endogenous latent growth factor complex, transforming growth factor–β1 (TGF-β1), that subsequently differentiates host stem cells to promote tissue regeneration. LPL treatment induced reactive oxygen species (ROS) in a dose-dependent manner, which, in turn, activated latent TGF-β1 (LTGF-β1) via a specific methionine residue (at position 253 on LAP). Laser-activated TGF-β1 was capable of differentiating human dental stem cells in vitro. Further, an in vivo pulp capping model in rat teeth demonstrated significant increase in dentin regeneration after LPL treatment. These in vivo effects were abrogated in TGF-β receptor II (*TGF-βRII*) conditional knockout (*DSPP^{Cre}TGF-βRII$^{fl/fl}$*) mice or when wild-type mice were given a TGF-βRI inhibitor. These findings indicate a pivotal role for TGF-β in mediating LPL-induced dental tissue regeneration. More broadly, this work outlines a mechanistic basis for harnessing resident stem cells with a light-activated endogenous cue for clinical regenerative applications.

INTRODUCTION

Regenerative medicine is currently focused on directing differentiation of stem cells into lineage-specific, functional cells that can promote tissue repair and organization. Stem cell therapies are attractive for treating numerous diseases, including dental diseases (for example, tooth decay and gum disease), which are among the most prevalent health concerns. Current clinical dentistry is predominantly focused on restorative approaches involving placement of inert materials, but tissue regeneration is an attractive alternative because materials alone fail with time and do not provide the full function of the tissue (*1*). Several different biological and biomechanical cues are presently being explored to direct stem cell behavior. Clinical application of stem cell therapies is exemplified by culture-based manipulation of patient-specific cells and reintroduction into specific anatomical contexts. In contrast, exogenous morphogens may be delivered to tissues to mobilize and promote resident stem cells toward specific biological functions. In either situation, exogenous materials must be delivered to the body with stringent spatial and temporal control, and this poses significant technical, regulatory, economic, and biological (off-target effects) barriers to widespread clinical applications (*2*).

Targeting resident stem cell pools by activating endogenous morphogens could potentially bypass many of the limitations of the current approaches to regenerative medicine and revolutionize the field (*3*). Among these endogenous factors, physiologically available latent growth factor complexes, such as members of the transforming growth factor–β (TGF-β) superfamily, could be harnessed as potent cues. TGF-β is secreted as a latent complex, and its activation is a key step in its physiological function (*4*). The TGF-β superfamily is encoded by 23 distinct genes that include *TGF-β*, *bone morphogenetic protein* (*BMP*), *Activin*, *Nodal*, *Inhibin*, and *growth differentiation factor* (*GDF*) (*5*, *6*). Their interactions and complex context-dependent roles in modulating stem cell pluripotency and differentiation have been elegantly demonstrated in a variety of experimental models. Recent studies highlight the role of the TGF-β signaling pathway as a master regulator of stem cell differentiation (*7*, *8*). The induction of *Oct4* and *Nanog* expression by specific inhibition of TGF-β receptor I (TGF-βRI) with subsequent absence of lineage differentiation marker expression has identified TGF-β signaling as a key player in stem cell pluripotency and differentiation (*9*–*11*). Moreover, TGF-βs have a central role in tooth development, specifically in the pulp-dentin pathophysiology that is used as the experimental model in this study, and are among the most promising cues in regenerative endodontics (*12*, *13*).

Several methods of latent TGF-β1 (LTGF-β1) activation have been described, including extreme pH, heat, ultrasound, integrin binding, ionizing radiation, and proteases, such as thrombospondin-1 (*14*). These TGF-β triggers have various degrees of attractiveness for clinical application because of practical and safety concerns. Light is an appealing modality for regenerative medicine, but its use to date has been predominantly focused on its destructive phototoxic effects, for example, to kill tumor cells. In contrast to those modalities, low-power light (LPL) therapy has been noted to reduce pain and inflammation and to promote wound healing, and these effects are collectively termed photobiomodulation

[1]Harvard School of Engineering and Applied Sciences, Cambridge, MA 02138, USA. [2]Wyss Institute for Biologically Inspired Engineering, Boston, MA 02115, USA. [3]Harvard School of Dental Medicine, Boston, MA 02115, USA. [4]Leder Human Biology and Translational Medicine, Boston, MA 02115, USA. [5]National Institute of Dental and Craniofacial Research, Bethesda, MD 20892, USA. [6]Wellman Center for Photomedicine, Massachusetts General Hospital, Boston, MA 02114, USA. [7]Children's Hospital Boston, Boston, MA 02115, USA. [8]Department of Dermatology, Harvard Medical School, Boston, MA 02115, USA. [9]Harvard-MIT Division of Health Sciences and Technology, Boston, MA 02139, USA. [10]New York University School of Medicine, New York, NY 10016, USA.
*Corresponding author. E-mail: mooneyd@seas.harvard.edu

(*15*). LPL treatment has been anecdotally noted to promote regeneration in cardiac, skin, lung, and nerve tissues (*16*). These regenerative responses have been suggested to be mediated by direct or indirect effects on stem cells (*17*–*19*), but a direct link between laser treatment and stem cell biology has not yet been clearly demonstrated.

Here, we evaluate the ability of LPL to direct differentiation of dental stem cells for dentin regeneration, and investigate the precise molecular mechanisms involved in the process. LPL appears to generate reactive oxygen species (ROS), which in turn activate LTGF-β1 via a specific methionine (position 253) on latency-associated peptide (LAP). A rodent pulp-dentin healing model was used in these studies owing to the abundant, endogenous adult dental stem cell population within the readily accessible oral cavity.

RESULTS

LPL treatment induces tertiary dentin formation

Tooth pulps in two rat maxillary first molars were mechanically exposed: one site received LPL treatment, whereas the other served as a

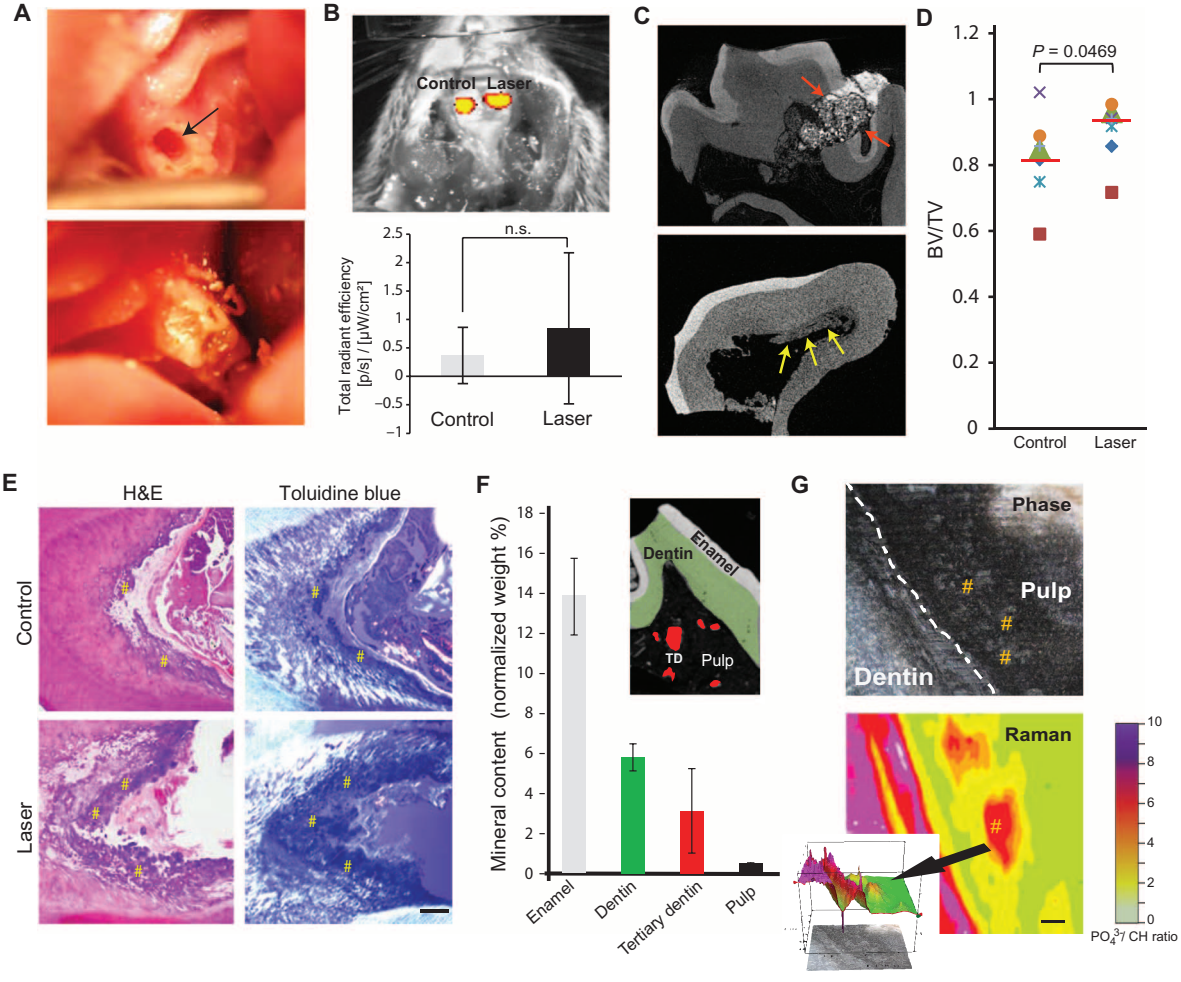

Fig. 1. LPL induces tertiary dentin in a rodent model. (**A**) An occlusal defect (arrow, top panel) exposed the pulp in the maxillary first molar in rats. These defects were subsequently irradiated with LPL, packed with microspheres or $Ca(OH)_2$ dressing, and sealed with a restoration (bottom panel). (**B**) Image and quantification of inflammatory response with a myeloperoxidase probe at 24 hours after pulpal exposure and restoration (Control) versus pulpal exposure followed by LPL treatment (Laser). Data are means ± SD ($n = 3$). $P > 0.05$, paired two-tailed t test. (**C**) Dentin repair imaged by high-resolution μCT. Red arrows in top panel indicate cement filling, and yellow arrows in lower panel indicate tertiary dentin deposition along walls of pulp chamber. (**D**) Quantification of mineralized tissue formation in defects after 12 weeks using high-resolution μCT imaging after pulp exposure alone (Control) and LPL treatment (Laser). Tissue formation defined by the ratio of bone volume (BV) to total tooth volume (TV). Data are individual animals represented by unique symbols ($n = 7$). Red lines denote means; P value determined by Wilcoxon matched-pairs signed rank test. (**E**) Histological analysis of decalcified teeth by hematoxylin and eosin (H&E) and toluidine blue staining, with polarized illumination. Sections were taken from tissue adjacent to the defect. # indicates regions of tertiary dentin. Scale bar, 200 μm. (**F**) Mineral content of nondecalcified sections by scanning electron microscopy (SEM)–EDS. Data are means ± SD ($n \geq 3$). Inset image depicts pseudocolored SEM image of regions assessed for analyses. TD, tertiary dentin. (**G**) LPL-treated nondecalcified tooth samples ($n = 2$) were imaged using Raman microscopy to see compositional map of ratio of phosphate (PO_4^{3-}) to CH. Scale bar, 100 μm. Inset shows quantitative histograph depicting spatial distribution of intrapulpal islands (arrow) of tertiary dentin induction. # indicates regions of tertiary dentin within the pulp.

control (no laser); both teeth received a filling (Fig. 1A). LPL treatment did not significantly affect the inflammatory response at 24 hours, as indicated by a myeloperoxidase probe (Fig. 1B and fig. S1A). Calcium hydroxide [$Ca(OH)_2$] dressing was used as a positive control for tertiary dentin induction in this model (fig. S1B). Tertiary dentin induction was assessed with high-resolution microcomputed tomography (μCT) (Fig. 1C). Increased tertiary dentin volumes were observed 12 weeks after LPL treatment compared to controls by μCT (Fig. 1D) and by histology (Fig. 1E and fig. S1C). Tertiary dentin is characterized by disorganized, bone-like (osteodentin) morphology and distinct mineral composition and anatomical location, as noted in the $Ca(OH)_2$-treated samples (fig. S2). LPL-induced tertiary dentin had a similar composition to that observed with $Ca(OH)_2$-treated samples as assessed with energy-dispersive spectroscopy (EDS) (Fig. 1F) and Raman microscopy (Fig. 1G).

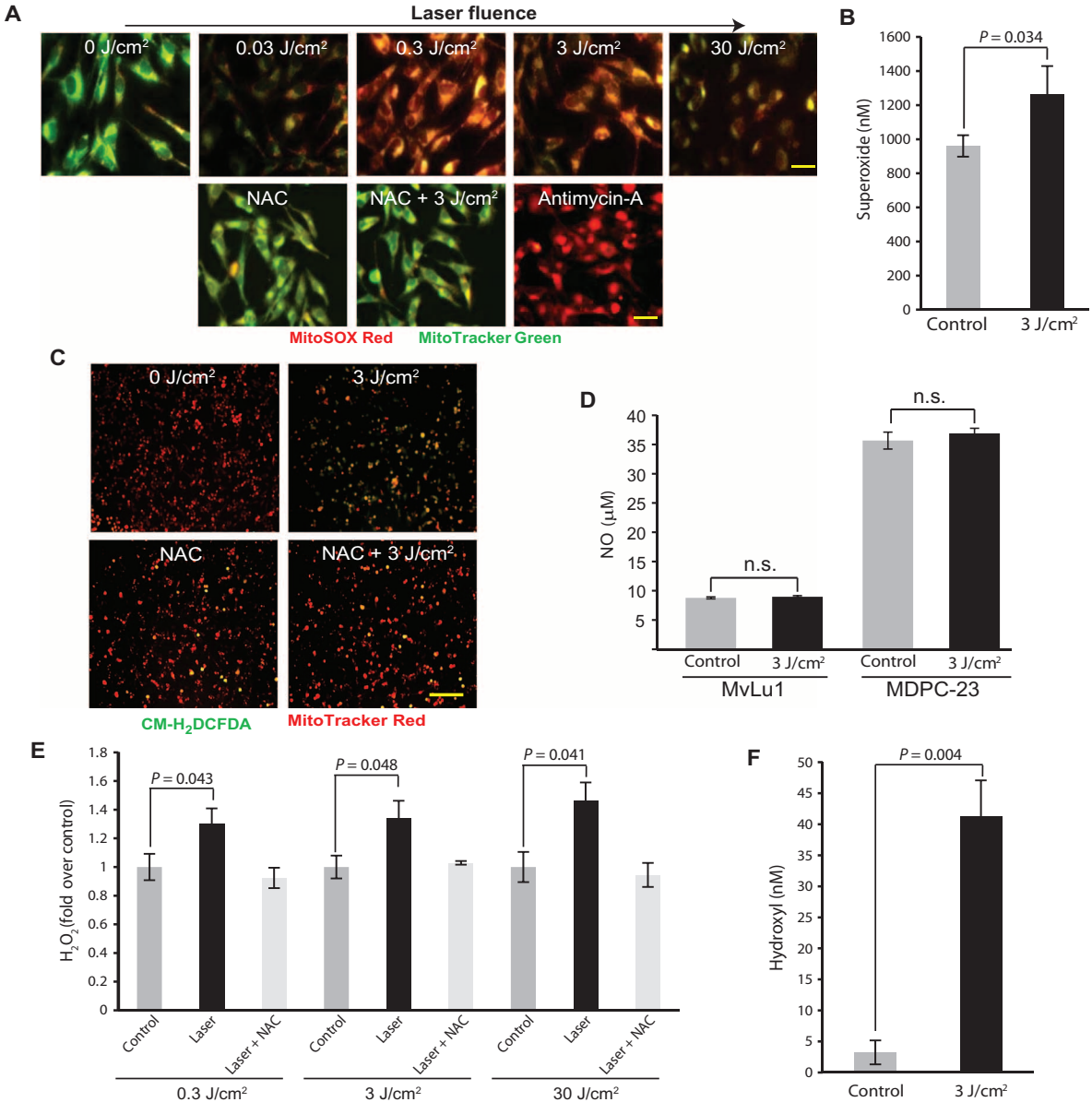

Fig. 2. LPL treatment generates ROS in mammalian cells in vitro. (**A**) Mv1Lu cells were treated with LPL at various fluences and assessed for superoxide generation with MitoSOX Red. Mitochondria were counterstained with MitoTracker Green. Red and green overlays are shown representative of three independent experiments. Some cells were preincubated with NAC (1 mM) before LPL (3 J/cm^2) treatment or antimycin A treatment as a positive control. Scale bars, 20 μm. (**B**) Superoxide generation after LPL (3 J/cm^2) treatment of Mv1Lu cells. Data are means ± SD (n = 3). P value determined by two-tailed t test. (**C**) H_2O_2 generation in Mv1Lu cells (revealed by CM-H_2DCFDA) in response to LPL irradiation, with or without NAC (1 mM). Mitochondria were counterstained with MitoTracker Red. Red and green overlays are shown. Scale bar, 100 μm. (**D**) Griess assay for NO generation after LPL (3 J/cm^2) treatment of Mv1Lu cells and mouse dental papilla cells (MDPC-23). (**E**) H_2O_2 generation assessed with Amplex UltraRed after LPL treatment of FBS at various fluences. Some samples were preincubated with NAC (1 mM) before LPL treatment. (**F**) LPL (3 J/cm^2)–induced generation of hydroxyl radicals in cell-free serum, as assessed with proxylhydroxylamine. In (D) to (F), data are means ± SD (n = 3). P values determined by two-tailed t test.

These findings indicate that LPL treatment induces tertiary dentin formation within the rat tooth pulp.

LPL treatment generates ROS

We next examined the mechanisms mediating the regenerative effects of LPL treatment. LPL-induced ROS generation was assessed using fluorescent probes (table S1). Increased superoxide and hydrogen peroxide (H_2O_2) were observed in mink lung epithelial cells (Mv1Lu) after LPL treatment in a dose-dependent manner, whereas no changes in nitric oxide (NO) were noted in either Mv1Lu or mouse dental pulp cells [mouse dental papilla cell-23 (MDPC-23)] (Fig. 2, A to D). Incubation with a ROS scavenger, *N*-acetyl cysteine (NAC), reduced ROS detection after LPL treatment (Fig. 2, A and C). Antimycin A, an inhibitor of mitochondrial oxidative phosphorylation that generates ROS, was used as a positive control.

Cell-free solutions of fetal bovine serum (FBS) were next subjected to LPL treatment. An LPL dose–dependent generation of superoxide, H_2O_2, and hydroxyl radicals was noted (Fig. 2, E and F, and fig. S3A). Substitution of water with deuterium, which enhances ROS lifetimes owing to differences in dielectric and diffusion constants, to dilute serum resulted in a significant increase in LPL-induced ROS (fig. S3B). Transition metals form core proton donor complexes that facilitate photon absorption. Depleting transition metal ions by preincubating serum with Chelex resin followed by LPL treatment demonstrated a significant reduction in ROS generation (fig. S3C).

LPL-ROS activates LTGF-β

Because LPL generates ROS in vitro, the role of these reactive intermediate chemical species in modulating biological complexes was explored further. Using a fluorescent dye, IAEDANS, that binds to free cysteines, we noted increased fluorescence after LPL treatment of FBS, indicating that LPL induces conformational changes of constituent serum complexes (Fig. 3A). To identify possible candidates, IAEDANS-labeled serum samples were subjected to gel electrophoresis, and distinct complexes were noted in the LPL-treated samples compared to the controls (Fig. 3B, left panel). One major band was serum albumin, which undergoes redox-sensitive conformational changes (*20*). Immunoblotting identified other bands as various forms of TGF-β (Fig. 3B, right panel), as expected from previous studies (*21*, *22*). Cleavage of disulfide linkages, exposing free cysteines (*23*), is involved in TGF-β1 activation; thus, this finding suggests that LPL treatment leads to TGF-β1 activation. Solutions of purified, recombinant human LTGF-β1 (rhLTGF-β1) were also tested, and results demonstrated that LPL treatment is capable of directly modulating its conformational structure (Fig. 3A).

The ability of LPL to directly activate LTGF-β1 was next characterized. Serum and recombinant LTGF-β1 were treated with LPL, and their activation was assessed by enzyme-linked immunosorbent assay (ELISA). LPL activated two different forms of LTGF-β1 in a dose-dependent manner (Fig. 3C and fig. S4A). Furthermore, LPL treatment of TGF-β reporter (p3TP-luc) MvLu1 cells led to increased luciferase activity (fig. S4B), indicating that LPL-activated TGF-β was biologically potent. Preincubation of these cells with inhibitors of ROS (NAC) or TGF-βRI (SB431542) before LPL treatment partially reduced luciferase reporter activity (fig. S4B). The inability of these inhibitors to provide complete loss of reporter activity is likely due to AP-1 (activator protein 1) elements in the p3TP reporter that are amenable to transactivation by other growth factors (*24*).

Individual ROS generated by LPL—namely, superoxide, H_2O_2, and hydroxyl radicals—were assessed for their ability to activate LTGF-β1. All three species were generated individually in serum (table S1) and were capable of activating the LTGF-β complex (fig. S4C). A critical TGF-β1 residue that confers ROS sensitivity is methionine at position 253 on the latency-associated peptide (LAP); mutation to alanine (M253A) abrogates this ROS sensitivity (*25*). Stably transfected mouse embryonic fibroblasts (MEFs) secreting either a full-length wild-type or a ROS-insensitive mutant (M253A) of LTGF-β1 were used to assess

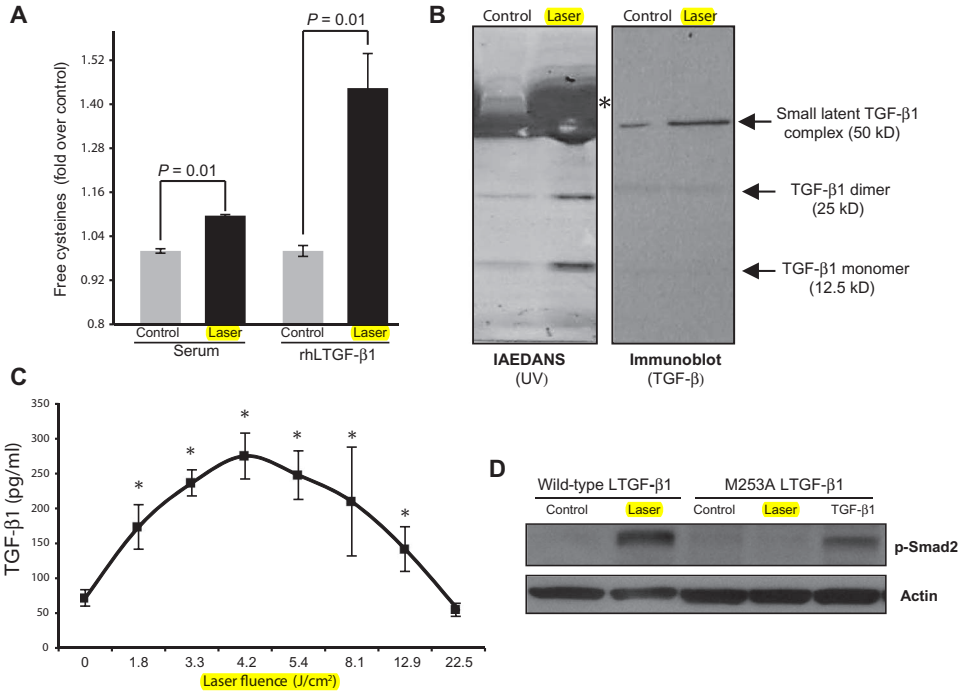

Fig. 3. LPL-generated ROS activates LTGF-β1 in vitro. (**A**) Free cysteines in serum and in a solution of rhLTGF-β1 after LPL treatment (3 J/cm^2). Data are means ± SD ($n = 3$). *P* values determined by two-tailed *t* test. (**B**) Control and LPL-treated serum samples were labeled with IAEDANS and then separated by gel electrophoresis; specific bands were visualized by ultraviolet, indicating the labeling of LPL-induced conformational changes in putative candidates. Right panel shows the same samples, transferred onto a nitrocellulose membrane and subjected to immunoblotting against TGF-β1. Asterisk indicates serum albumin. (**C**) TGF-β1 activation in serum after treatment with LPL at increasing fluences assessed with ELISA. Data are means ± SD ($n > 3$). *P* value was determined by two-tailed *t* test with Bonferroni correction compared to control (no laser treatment). (**D**) Phosphorylated Smad2 after LPL treatment of wild-type MEFs or MEFs transfected with mutated (M253A) LTGF-β1. Mutated MEFs were also treated with recombinant TGF-β1 to ensure signaling competency (without laser treatment).

LPL-generated ROS activation of LTGF-β1. Both cell lines secreted equivalent levels of LTGF-β1 and were amenable to routine chemical activation (fig. S4D). On treatment with LPL, the MEFs expressing wild-type LTGF-β1 demonstrated a robust increase in p-Smad2, but this was absent in MEFs with mutant LTGF-β1 (Fig. 3D). Direct addition of recombinant TGF-β1 to the mutant MEFs induced p-Smad2, confirming the integrity of the TGF-β signal transduction pathway in these cells. Treatment of conditioned medium from mutated MEFs with H_2O_2 also demonstrated decreased TGF-β activation, as compared to medium from wild-type MEFs (fig. S4, D and E). Together, these results indicate that ROS sensitivity in the LAP is required for TGF-β activation by LPL treatment.

LPL treatment directs differentiation of human dental stem cells

We next investigated possible biological targets of the LPL–ROS–TGF-β1 axis in the context of tooth regeneration. TGF-β has a central role in mediating mammalian odontoblast differentiation (*26*, *27*). Adult human dental stem cells (hDSCs) in the tooth pulp express characteristic stem cell surface markers (positive for CD44, CD90, CD106, CD117, and Stro-1; negative for CD45) and are capable of multilineage differentiation, making them key players in tooth regeneration (*28*). The ability of LPL to activate TGF-β1 and direct the differentiation of these dental stem cells was thus examined. hDSCs were isolated from extracted tooth specimens, and the expression of pluripotency cell surface markers was confirmed (fig. S5). LPL activated TGF-β1 in the hDSCs (Fig. 4, A and B), which was blocked with NAC or SB431542. LPL treatment demonstrated substantial down-regulation of stem cell markers Stro-1, CD90, CD117, and CD44, whereas CD106 expression was slightly reduced (Fig. 4, C and D). This suggests that LPL induced a transition in these cells away from their pluripotent state. Concurrently, LPL-treated stem cells exhibited an increase in markers of odontoblast (dentin-forming cells) differentiation compared to control hDSCs, including dentin matrix protein 1 (DMP1), dentin sialoprotein (DSP), osteopontin (OPN), and alkaline phosphatase (ALP) (Fig. 4E) (table S2) (*29*, *30*).

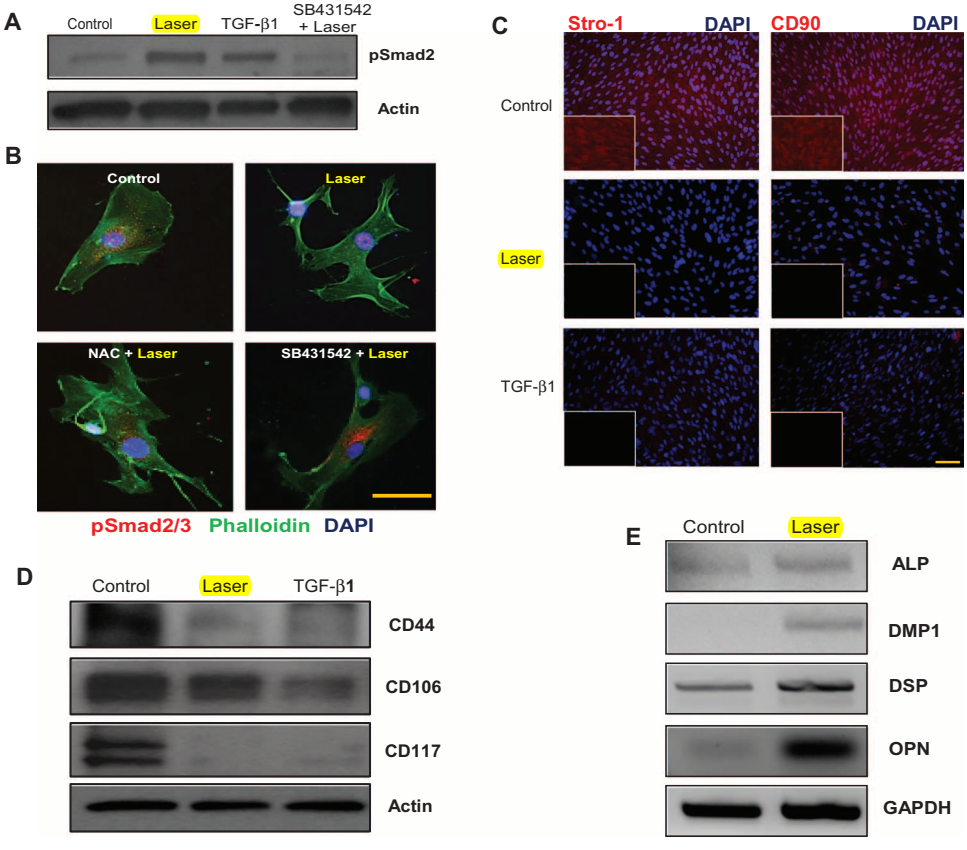

Fig. 4. LPL-induced odontoblastic differentiation of human dental stem cells (hDSCs). (**A**) Phospho-Smad2 expression in hDSCs after LPL treatment. TGF-β1 treatment served as a positive control. Some cells were pretreated with TGF-βRI inhibitor, SB431542, before LPL treatment. Actin served as a loading control. (**B**) The TGF-β responsiveness of hDSCs was assessed by nuclear translocation of p-Smad2/3 after LPL treatment. Counterstaining for cytoskeletal actin (phalloidin) and nuclei [4′,6-diamidino-2-phenylindole (DAPI)] was performed. Tricolor overlays are shown. Some samples were preincubated with NAC or SB431542 before LPL treatments. Scale bar, 20 μm. (**C**) Immunofluorescent labeling of stem cell markers Stro-1 and CD90 in hDSCs 7 days after LPL or TGF-β1 treatment. Controls are untreated hDSCs. Nuclei were counterstained with DAPI. Inset shows red channel only. Scale bar, 50 μm. (**D**) Western blots for stem cell markers CD44, CD106, and CD117 in hDSCs 7 days after LPL or TGF-β1 treatment. Actin served as a loading control. (**E**) Dentin matrix expression was assessed by semiquantitative reverse transcription polymerase chain reaction (RT-PCR) in hDSCs, 7 days after LPL treatment. Gel images were inverted (black bands) for clarity of presentation.

LPL induces dentin differentiation in two- and three-dimensional cultures

To further confirm the role of LPL in odontoblast differentiation, a mouse preodontoblast cell line, MDPC-23, was subjected to LPL treatments. LPL activated TGF-β signal transduction and induced ALP activity in these cells in two-dimensional (2D) culture (Fig. 5, A and B). This appeared to be partly mediated by ROS and TGF-β, as preincubation with NAC or SB431542 partially reduced ALP activity (Fig. 5B and fig. S6A). Owing to limited spatial differentiation, matrix secretion, and organization in 2D culture systems, a poly(lactide-*co*-glycolide) (PLG) scaffold system was used to assess mature dentin differentiation in 3D (Fig. 5C). LPL treatment activated TGF-β1 in the 3D scaffold system, as observed with increased luciferase activity in TGF-β reporter (p3TP-luc) MvLu1 cells (Fig. 5D). TGF-β signaling was prevented by preincubation with NAC, indicating that LPL-generated ROS are necessary. As a positive control, addition of recombinant TGF-β1 itself robustly induced luciferase activity.

MDPC-23 cells were cultured in the 3D PLG scaffolds under mineralizing culture conditions for 21 days. Supplementing cultures with recombinant TGF-β1 or treating cells with conditioned medium activated with H_2O_2 induced dentin matrix expression and ALP activity (fig. S6, B and C). LPL treatment induced dentin differentiation in 3D culture, as indicated by up-regulation of ALP activity and DMP1 and OPN expression (Fig. 5, E and F). Together,

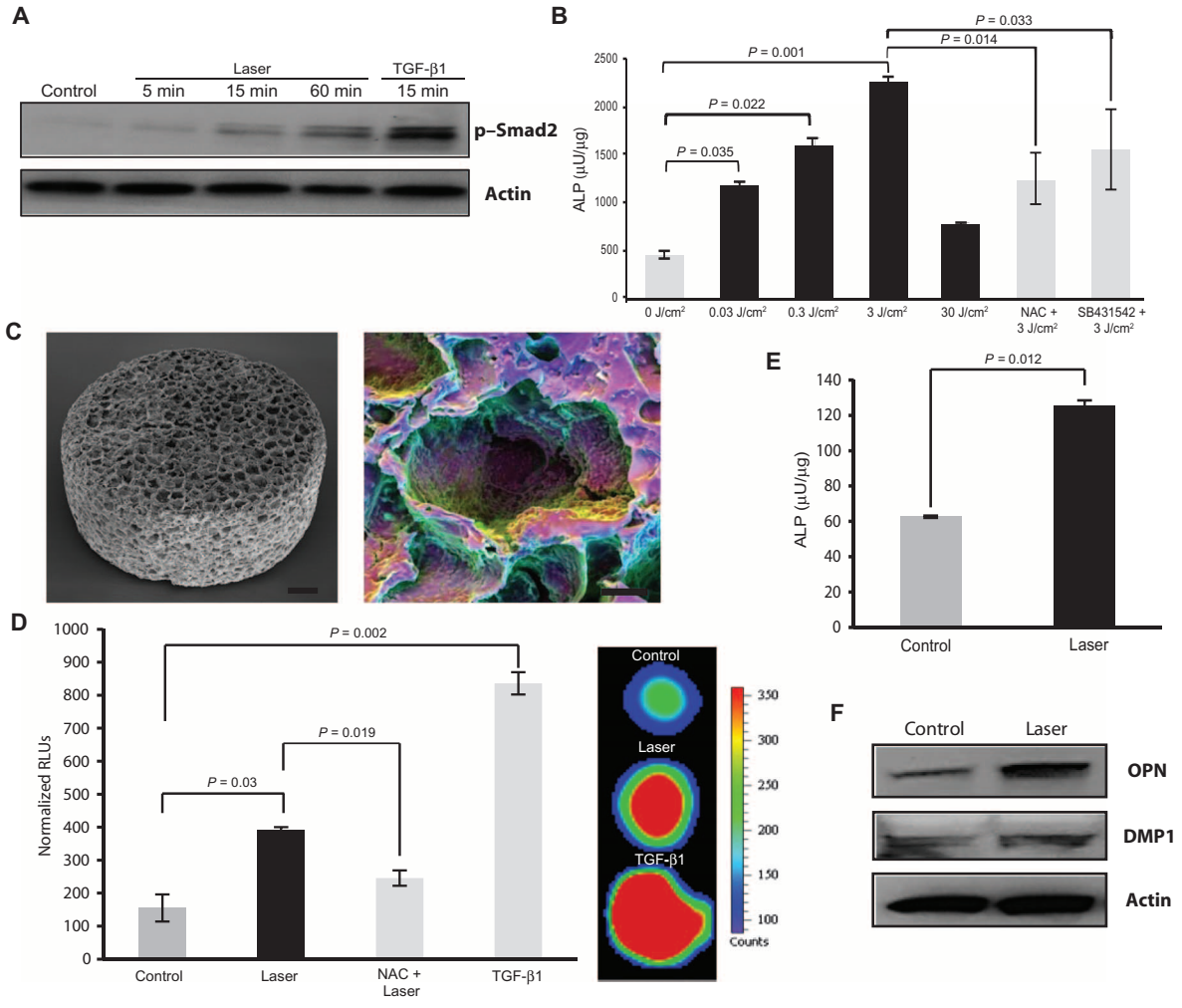

Fig. 5. LPL directs dentin differentiation in 2D and 3D mouse pre-odontoblast cultures. (**A**) The kinetics of TGF-β1 responsiveness of MDPC-23 after LPL or TGF-β1 treatment was assessed with phospho-Smad2 Western blot. (**B**) ALP activity 3 days after LPL treatment of mouse MDPC-23 cells. Some cells were preincubated with NAC or SB431542 before LPL treatments. (**C**) SEM image of PLG macroporous scaffolds used for 3D culture (left). Polychromatic SEM technique shows cells seeded within scaffold pores (right). Scale bars, 100 μm (left) and 50 μm (right). (**D**) Left panel shows quantification of luciferase activity from TGF-β reporter (p3TP luc) Mv1Lu cells at 24 hours after LPL or TGF-β1 treatment. Some scaffolds were preincubated with NAC before LPL treatment. Panel on the right shows hypercolored image of in situ luciferase imaging of reporter cells within 3D scaffolds. (**E**) LPL induction of mineralizing phenotype assessed by ALP activity in mouse odontoblast-like cells (MDPC-23) cultured in 3D scaffold cultures at 21 days. (**F**) Western blots for DMP1 and OPN after LPL treatment of MDPC-23 cells cultured in 3D PLG scaffolds for 21 days. In (B), (D), and (E), data are means ± SD ($n = 3$). P values determined by two-tailed t test.

these observations suggest that LPL treatment directs dentin differentiation of hDSCs (2D culture) and mouse pre-odontoblasts (2D and 3D culture) via the ROS–TGF-β axis.

TGF-β1 is critical for LPL-mediated dentin regeneration in vivo

Two distinct interventional strategies were chosen to confirm the in vivo role of LPL-activated endogenous TGF-β1 in dentin regeneration. In the first approach, LPL treatment was combined with controlled delivery of a small-molecule inhibitor of TGF-βRI (Alk5), SB431542, from PLG microspheres on the exposed dental pulp of rat teeth (fig. S7). Sustained release of TGF-βRI inhibitor at the site of LPL treatment over the course of 7 days prevented tertiary dentin induction, as observed with μCT and histology (Fig. 6, A and B), supporting the role of TGF-β in LPL-mediated regeneration.

The second in vivo approach was taken using transgenic mice. A conditional knockout ($DSPP^{Cre}TGF\text{-}\beta RII^{fl/fl}$) mouse was generated by crossing dentin sialophosphoprotein-Cre ($DSPP^{Cre}$) with the floxed TGF-β type II receptor ($TGF\text{-}\beta RII^{fl/fl}$) mice (fig. S8, A and B). The *DSPP* gene is expressed in late dentinogeneses and encodes two distinct dentin matrix proteins with key roles in dentin mineralization, namely, DSP and dentin phosphoprotein (DPP) (*31*). TGF-βRII is the specific receptor for TGF-β ligands and has very high affinity for TGF-β isoforms 1, 2, and 3 (*32*). The *TGF-βRII* knockout mouse simulates *TGF-β* knockout, indicating that it has a key role in normal TGF-β pathophysiology (*33*). $DSPP^{Cre}$ was noted to be expressed postnatally (fig. S8, C and D), and the $DSPP^{Cre}TGF\text{-}\beta RII^{fl/fl}$ mice appear to have normal dentin morphology and organization (fig. S8, E and F). Moreover, tooth pulp cells from the $DSPP^{Cre}TGF\text{-}\beta RII^{fl/fl}$ mice were capable of a mineralized tissue repair

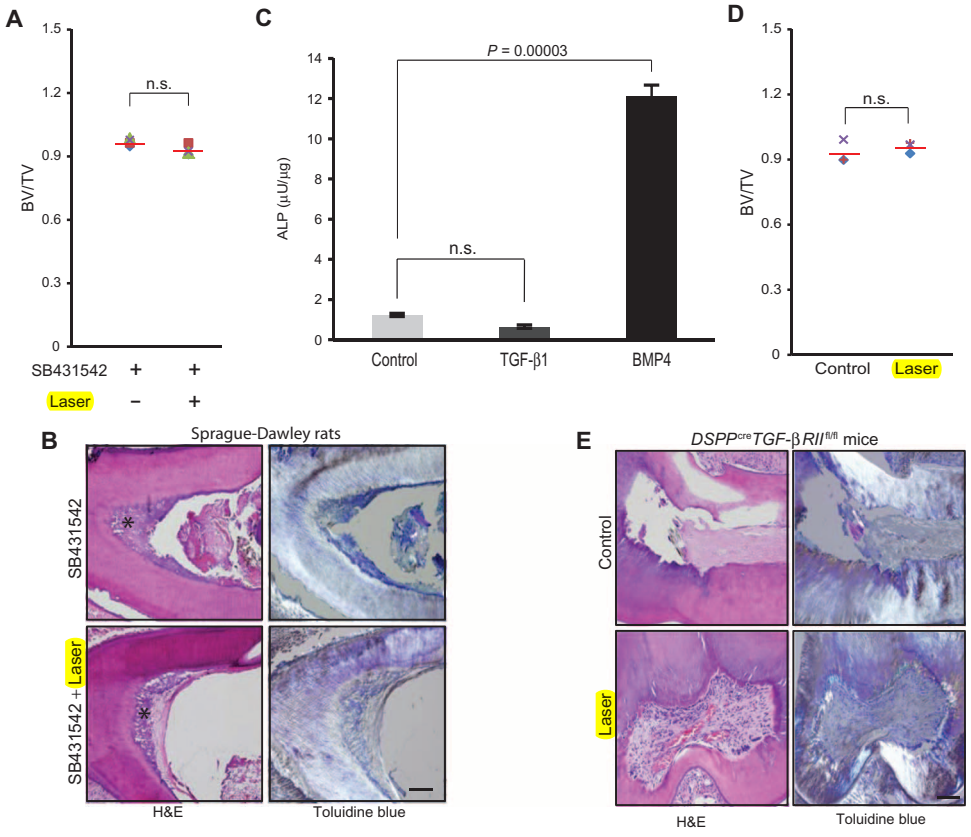

Fig. 6. TGF-β mediates the effect of LPL on dentin formation in vivo. (**A**) Quantitation of induced tertiary dentin volume, as indicated by the ratio of bone volume (BV) to total tooth volume (TV), of rats treated with SB431542 alone or with LPL treatment assessed by μCT at 12 weeks. Means (red lines) are presented; each data point represents individual animal (n = 4). P value determined by Wilcoxon matched-pairs signed rank test. (**B**) H&E and toluidine blue staining, with polarized illumination, of tooth sections obtained from rats treated with SB431542 (TGF-βRI inhibitor) with or without LPL. Scale bar, 200 μm. Asterisk denotes tertiary dentin noted along the pulp walls. (**C**) Pulp cells from *DSPP*^{Cre}*TGF-βRII*$^{fl/fl}$ teeth were treated with TGF-β1 and BMP4 and assessed for ALP activity. Data are means ± SD (n = 4). P values determined by two-tailed t test. (**D**) Quantitation of dentin volume in teeth of *DSPP*^{Cre}*TGF-βRII*$^{f/f}$ mice with no treatment (Control) or after LPL treatment (Laser) at 8 weeks. Means (red lines) are presented; each data point represents an individual animal (n = 3). P value determined by Wilcoxon matched-pairs signed rank test. (**E**) H&E and toluidine blue staining, with polarized illumination, of tooth sections obtained from *DSPP*^{Cre}*TGF-βRII*$^{fl/fl}$ mice that were either untreated (Control) or LPL-irradiated (Laser). Scale bar, 200 μm.

response (BMP4-induced ALP activity), but were nonresponsive to TGF-β1 stimulation (Fig. 6C).

LPL treatment of exposed pulp in the *DSPP*^{Cre}*TGF-βRII*$^{fl/fl}$ mice (n = 3) demonstrated similar amounts of tertiary dentin induction to untreated controls by μCT analyses (Fig. 6D). Histological analyses of teeth from both groups demonstrated minimal dentin induction (Fig. 6E). The LPL-treated teeth also demonstrated engorged, dilated blood vessels with better organized stroma (Fig. 6E). This could be potentially attributed to differences in sectioning planes. In contrast, a normal dentin repair response was noted in *TGF-βRII*$^{fl/fl}$ mice (n = 2), similarly in rats (Fig. 1), after LPL treatments (fig. S9). These two distinct in vivo approaches targeting the TGF-β pathway in both rat and mouse teeth support the role of endogenous TGF-β activation in mediating LPL regenerative effects on tertiary dentin induction.

DISCUSSION

A wide variety of biochemical (small molecules, growth factors, peptides, microRNAs) and biophysical (electrical, magnetic, ultrasound) cues are currently being explored for their ability to promote tissue regeneration. The ability of LPL to activate an endogenous morphogen to direct resident stem cell differentiation—in this case, dental stem cell—adds a new, potent tool to the regenerative armamentarium. This study elucidated both the efficacy and the primary mechanistic role of LPL and ROS–TGF-β1 in mediating dentin regeneration. The ability to activate endogenous components in a controlled, self-limiting manner is a critical aspect of this potential therapeutic modality because both ROS and TGF-β1 in excessive amounts are potently deleterious (*34*, *35*). The absolute LPL-activated levels of both these key intermediates would depend on their biological source and presence of other inhibitors (for example, antioxidants) in the treatment zones. Our simplest cell-free system with serum solutions was meant to test the post-wounding hemostatic milieu, present during LPL treatment, containing abundant platelet-derived and serum LTGF-β1. Nonetheless, LPL treatment extends well beyond the local exposure site and could potentially activate other sources, such as cell-secreted and extracellular matrix– and dentin matrix–sequestered forms of LTGF-β1 (*36*). TGF-β has key roles in many biological processes including development, immune responses, wound healing, and malignancies (*37*). Modulating endogenous LTGF-β, as shown in this study, could provide a powerful tool to study its role in normal physiology and pathology and could be exploited therapeutically in many of these contexts.

It is prudent to note that the mineralized tissue (tertiary dentin) induction was noted in a widespread area within the pulp after LPL treatment, leading to formation of pulp stones, rather than an ideal reparative dentin bridge. This was probably a result of the large area of laser–biological tissue interactions and the paracrine effects of the activated factor. Good operative techniques that minimize both the exposed pulp surface and mechanical debris have been shown to be key factors in determining dentin regeneration (*38*). Therefore, better surgical techniques, which are possible in larger animals and humans, as well as optical focusing approaches, such as multiphoton modalities, are likely to allow one to restrict laser-biological interactions to the treatment interface and to improve LPL therapeutic efficacy. Further, it is important to highlight that the long-term effects on mineralized tissue regeneration in this study were initiated by a single LPL treatment; multiple clinical

treatment dosing protocols could lead to more profound, optimized therapies. Limitations of this study are the small sample sizes in the mouse studies, owing to limited availability of these transgenic animals, and technical difficulties of instrumenting minute tooth samples and maintaining their integrity during processing.

Lasers are widely used in various biomedical applications (for example, microscopy and spectroscopy), and clinical high-power laser applications are common in ophthalmology, surgery, and dermatology. The use of lasers for in vivo optical imaging is also gaining rapid popularity with techniques such as optical coherence tomography and laser speckle imaging. These latter optical imaging applications also use very low doses of photoillumination, raising interesting questions on their potential therapeutic side effects. The major purpose of this study was to explore the primary molecular mechanisms underlying near-infrared, LPL treatment–induced regeneration. Studies on the molecular mechanisms mediating photobiomodulation or low-level light therapy have previously focused on in its role in modulating the mitochondrial enzyme, cytochrome c oxidase, and ROS generation (*39*). Recently, a potent role of ROS in mediating regeneration has been described (*40*). Although the precise nature of the LPL photoabsorber remains unclear in our current study, the results in this study suggest a critical role for metal ions and water molecules; the photoabsorber may absorb photons to form an excited triplet state, which further undergoes energy transfer with oxygen to form various ROS. The expanding applications of lasers in medicine highlight the importance of understanding photon-biological interactions.

Regenerative medicine currently relies predominantly on ex vivo manipulated cells or the delivery of exogenous factors such as recombinant growth factors (*41*, *42*), and both approaches have significant limitations. The results of the current study suggest that a minimally invasive treatment, LPL, can be used to activate endogenous cues that can drive a regenerative response of resident stem cells, potentially bypassing the need to deliver exogenous cells or factors. These observations in multiple models (mice, rats, and primary hDSCs) suggest that this mechanism is conserved across species. This, combined with the simplicity of the LPL treatment, suggests that clinical translation would be straightforward. Given the broad range of roles that ROS and TGF-β can mediate in vivo and the popularity of laser devices in current clinical settings, the mechanistic insights from this study could also promote clinical translation of LPL treatments to modulate pain, inflammation, or immune responses, and promote tissues regeneration of bone, neural, vascular, and muscle tissues.

MATERIALS AND METHODS

Study design

hDSCs and a rodent pre-odontoblast cell line were chosen to recapitulate lineage-specific cell responses after laser treatments. Cell-free serum was used to assess LTGF-β1 activation because serum is abundant in the hemostatic milieu after injury (pulp exposure). The in vivo rodent direct pulp capping models were used to recapitulate routine human dental clinical scenarios after excavation of deep carious lesions. The conditional knockout studies were aimed at assessing if LPL treatment effects were mediated via TGF-β in vivo by generating a nonresponding dentin forming cell population. Two experimental sites were randomly assigned to control or test (LPL treatment) groups in each animal to allow paired comparisons. Analyses were performed in a nonblinded manner; teeth were analyzed immediately after retrieval and the same individual performed the LPL treatment and μCT analysis (P.R.A.). Multiple assays, including in vivo and in vitro imaging and molecular and biochemical analyses, used in this study were aimed at assessing two key endpoints in clinically successful dentin repair, namely, dentin-specific matrix expression and subsequent mineralized tissue repair.

Rodent model for dentin repair

Rats (Sprague-Dawley, 4 weeks, Charles River) and mice [4 to 6 weeks, C57B6/129SVJ/FvBN, National Institute of Dental and Craniofacial Research (NIDCR)] were used as rodent models of dental pulp repair as described previously (*43*). All procedures were approved by the Harvard University and NIDCR animal care and use care committees. Briefly, rats or mice were anesthetized [ketamine (80 to 120 mg/kg) and xylazine (5 to 10 mg/kg), intraperitoneally] and two cavity preparations were made on the occlusal aspect, exposing the pulp of the first maxillary molar tooth with a conventional handpiece (NSK), #1 round carbide bur (0.8 mm) (Dentsply), and portable dental unit (Dentport Dental Supply). Laser treatments were performed with an 810-nm GaAlAs laser diode system as described below. For loss-of-function studies in rats, two maxillary molar teeth were instrumented; pulp was exposed and packed with TGF-βRI inhibitor–releasing microspheres followed by a restoration. On the following day, the two teeth were re-instrumented exposing the pulp; one site received LPL treatment, and both sites were refilled with inhibitor microspheres and restored.

Cell culture

hDSCs and mouse pulp cells from $DSPP^{Cre}TGF\text{-}\beta RII^{fl/fl}$ mice were isolated from the pulp from tooth samples obtained, following Institutional Review Board approval at the Children's Hospital Boston, as previously described (*44*). Briefly, tooth specimens were dissected aseptically and incubated with 4 ml of 0.25% trypsin-EDTA (Life Technologies) at 37°C for 30 min. After neutralization with 4 ml of complete medium, solutions were pipetted vigorously to release cells and then passed through a cell strainer (70 μm, Corning), and resulting cells were cultured in complete medium supplemented with ascorbic acid (100 μM) and β-mercaptoethanol (50 μM) (both from Sigma). Mv1Lu (mink lung epithelial cells) (a gift from D. Rifkin, New York University, Langone Medical Center), MDPC-23 (mouse dental papilla cells) (a gift from T. Bottero, University of Michigan), D1 (mouse mesenchymal stem cells), and 7F2 (mouse osteoblasts) (both from American Type Culture Collection) cells were cultured in complete medium composed of 10% FBS, Dulbecco's modified Eagle's medium, GlutaMAX, and penicillin (100 U/ml)–streptomycin (100 μg/ml) (all from Gibco, Life Technologies) in a 37°C incubator with 5% CO_2. MEFs, stably transfected with either full-length or ROS-insensitive (M253A) LTGF-β1, were maintained in growth medium supplemented with G418 (Gibco, Life Technologies).

LTGF-β1–transfected MEFs

MEFs expressing either wild-type or M253A (ROS-insensitive mutant) LTGF-β1 were allowed to become 80% confluent in 10-cm dishes (Nunc, Thermo Fisher Scientific) and switched to 0.2% serum for medium conditioning. The medium from some dishes was assessed for total TGF-β1 (routine chemical activation: 1 N HCl for 10 min followed by 1.2 N NaOH and 0.5 M Hepes for 10 min) and H_2O_2 (100 μM) activation of LTGF-β1 with ELISA. In other plates, LPL treatment at 3 J/cm^2 was performed, and after 15 min, cells were washed with phosphate-buffered

saline, lysed, and subjected to immunoblotting for phospho-Smad2. As controls in these experiments, recombinant (active) TGF-β1 (2.5 ng/ml) (R&D Systems) was added to both cells to ensure signaling competency. In some cases, conditioned medium was removed and treated with H_2O_2 (100 μM) for 5 min before being added back to these cells.

Detection of ROS in the presence of cells

Cells were seeded in eight-well chamber slides (Nunc, Thermo Fisher Scientific) in complete medium and allowed to attach overnight. The following day, LPL treatment was performed at varying fluences, and cells were probed with fluorescent dyes to assess specific ROS, namely, MitoSOX Red dye (5 μM) for superoxide and CM-H_2DCFDA (10 μM) for H_2O_2. For both experiments, MitoTracker Green (500 nM) and MitoTracker Red (500 nM) (both from Molecular Probes, Life Technologies) were used to counterstain mitochondria. Fluorescence was visualized using a confocal microscope (Olympus IX81) and imaging software IP lab (version 4.0). The Griess assay (Promega) was performed per manufacturer's protocol. Briefly, cells were incubated with 50 μl of sulfanilamide for 10 min, followed by *N*-1-napthylethylenediamine dihydrochloride (NED) under acidic conditions for another 10 min. Absorbance was measured at 520 nm using a microplate reader.

Western blotting

Cells were lysed in radioimmunoprecipitation assay buffer (Sigma) with Complete Mini Protease Inhibitor (Roche). Lysates from MDPC-23 cells seeded in PLG scaffolds and rat dental pulp tissue were prepared by mincing with scissors in lysis buffer. This was followed by repeated sonication (Sonics) in lysis buffer on ice. Lysates were centrifuged at 14,000 rpm at 4°C for 20 min, and total protein was estimated with a Bradford assay (BCA, Thermo Scientific Inc.). Protein lysates were separated in precast tris-glycine or tris-acetate gels and transferred onto nitrocellulose membranes (both Invitrogen). Blots were incubated with various primary antibodies (table S3) at 4°C overnight. After washes, blots were incubated with appropriate species-specific secondary antibodies (Jackson ImmunoResearch Laboratories), and chemiluminescence (Thermo Scientific Inc.) was detected by films (Kodak MR, Sigma-Aldrich). Images were scanned digitally; brightness and contrast were adjusted for the whole image wherever appropriate.

Laser treatments

In vitro assays. A near-infrared laser was used in all experiments. Specifically, an 810-nm GaAlAs laser diode system (driver, temperature controller, and cooling mount) with a fiber optic delivery system (400 μm fiber) (all from Newport) was used in continuous wave mode. Laser dose was checked before each experiment with a power meter (Newport). Power density (irradiance, W/cm^2) was varied to achieve various energy densities (fluence, J/cm^2) for treating samples. For example, a spot size of 20, 30, or 50 mm for four wells in a 96-well plate, one 35-mm dish, or one 60-mm dish, respectively, was used by varying the target distance (beam divergence, 15°) and adjusting power (irradiance, W/cm^2) assessed with a power meter. All treatments were performed as described earlier, and treatment time (5 min) was kept constant in all experiments. Owing to variations in laser output at very low power levels and attenuation by cell culture plastic and medium, a 10% dose variance was included in all in vitro experiments. Cell-free solution experiments were performed in black wells, whereas cell treatments were performed with a black background (card sheet) placed below the clear-bottom culture dishes or wells.

In vivo assays. The same laser unit described above (Newport) was used for in vivo (mouse and rat) experiments. This unit has a 400-μm fiber delivery system, and the end piece was placed directly on the exposed pulpal tissue and used at 0.01 W/cm^2 for 5 min in continuous mode for a total dose of 3 J/cm^2. The end piece was moved continuously in a smooth, uniform motion during treatments to ensure that there was no appreciable heating. Animals were treated only once and followed for 8 weeks (mice) or 12 weeks (rats).

Generation and characterization of conditional knockout (*DSPP^{Cre}TGF-βRII$^{fl/fl}$*) mice

DSPP^{Cre} mice (*45*) were bred with *TGF-βRII$^{fl/fl}$* mice (*33*) to generate *DSPP^{Cre}TGF-βRII$^{fl/fl}$* mice and characterized by genotyping (table S2), histology, and μCT, as described in Supplementary Methods.

Pre-odontoblasts in 3D scaffold cultures

Mouse MDPC-23 cells (3 × 10^6 cells/ml) were seeded in PLG scaffolds (supporting methods) in complete medium. Cells were allowed to attach for 30 min and then floated in complete medium. After overnight incubation, LPL (above section) or TGF-β1 (2.5 ng/ml) treatments were performed. Scaffolds were placed in fresh medium in a 12-well plate with mineralizing supplements (10 mM β-glycerophosphate, 10 nM dexamethasone, and 20 mM ascorbic acid). The medium was changed every 3 days and maintained in culture for 21 days. Cell lysates from scaffolds were analyzed for ALP activity and dentin matrix induction.

Histological analyses

The tooth samples were decalcified and processed routinely for paraffin-embedded 4-μm serial sections. Owing to the tiny (0.7 to 1 mm) size of the tooth samples and relatively large defect created, sections at the defect site had poor integrity and were difficult to process for histology. Therefore, we chose to perform quantitative high-resolution μCT of the entire tooth to bypass these technical limitations (Supplementary Methods). For qualitative histological analysis, tissue sections adjacent to the defect (where remnants of filling materials were evident) were used. These sections were stained with H&E, Masson's trichrome, Azan Blue, and toluidine blue and examined with routine microscopy or polarized illumination (Nikon).

Statistical analyses

Data were analyzed using Microsoft Excel and GraphPad Prism software. Means and SDs were calculated. A Student's *t* test was performed for all data, unless otherwise noted, where $P < 0.05$ was considered statistically significant. In assays comparing multiple means, Bonferroni correction was applied. For the in vivo experiments, analyses were performed in a paired manner as two sites (molar teeth) in each animal were randomly assigned to either control or LPL treatment. Given the limited number of data points to assess data distribution in a valid manner, data were assumed to be distributed in a non-Gaussian manner and the nonparametric Wilcoxon matched-pairs signed rank test was used to analyze the data; $P < 0.05$ was considered statistically significant. The sample size for animal studies was based on previous studies reported in the literature, and power analyses (80% confidence interval, $\alpha = 0.05$, to detect a 10% change between treatment and control groups with an SD of 0.05) yielded a sample size $n = 4$. Owing to the limited availability of the transgenic mice and the technical difficulties of instrumenting minute mouse teeth effectively and maintain-

ing their integrity during processing, we were unable to power mouse studies adequately for statistical analysis in certain figures (Fig. 6D and fig. S9).

SUPPLEMENTARY MATERIALS

www.sciencetranslationalmedicine.org/cgi/content/full/6/238/238ra69/DC1
Materials and Methods
Fig. S1. Characterization of tertiary dentin induction by histology and μCT.
Fig. S2. Raman mapping for compositional assessment of tooth mineralized tissue.
Fig. S3. LPL-generated ROS in a cell-free system.
Fig. S4. LPL activation of LTGF-β1 is mediated by ROS.
Fig. S5. Characterization of hDSCs.
Fig. S6. Culture system for evaluation of the LPL–ROS–TGF-β1 axis.
Fig. S7. Release kinetics of TGF-βRI inhibitor from microspheres.
Fig. S8. Characterization of *DSPP*^{Cre}*TGF-βRII*$^{fl/fl}$ conditional knockout mice.
Fig. S9. LPL treatment of *TGF-βRII*$^{fl/fl}$ wild-type mice.
Table S1. Reagents used to generate and detect ROS.
Table S2. Primers and conditions for semiquantitative RT-PCR.
Table S3. List of antibodies for immunoassays.

REFERENCES AND NOTES

1. P. E. Murray, F. Garcia-Godoy, K. M. Hargreaves, Regenerative endodontics: A review of current status and a call for action. *J. Endod.* **33**, 377–390 (2007).
2. D. E. Discher, D. J. Mooney, P. W. Zandstra, Growth factors, matrices, and forces combine and control stem cells. *Science* **324**, 1673–1677 (2009).
3. Y. Xu, Y. Shi, S. Ding, A chemical approach to stem-cell biology and regenerative medicine. *Nature* **453**, 338–344 (2008).
4. Z. Yang, Z. Mu, B. Dabovic, V. Jurukovski, D. Yu, J. Sung, X. Xiong, J. S. Munger, Absence of integrin-mediated TGFβ1 activation in vivo recapitulates the phenotype of TGFβ1-null mice. *J. Cell Biol.* **176**, 787–793 (2007).
5. A. B. Roberts, M. A. Anzano, L. C. Lamb, J. M. Smith, M. B. Sporn, New class of transforming growth factors potentiated by epidermal growth factor: Isolation from non-neoplastic tissues. *Proc. Natl. Acad. Sci. U.S.A.* **78**, 5339–5343 (1981).
6. H. L. Moses, E. L. Branum, J. A. Proper, R. A. Robinson, Transforming growth factor production by chemically transformed cells. *Cancer Res.* **41**, 2842–2848 (1981).
7. A. C. Mullen, D. A. Orlando, J. J. Newman, J. Lovén, R. M. Kumar, S. Bilodeau, J. Reddy, M. G. Guenther, R. P. DeKoter, R. A. Young, Master transcription factors determine cell-type specific responses to TGF-β signaling. *Cell* **147**, 565–576 (2011).
8. Q. Xi, Z. Wang, A. I. Zaromytidou, X. H. Zhang, L. F. Chow-Tsang, J. X. Liu, H. Kim, A. Barlas, K. Manova-Todorova, V. Kaartinen, L. Studer, W. Mark, D. J. Patel, J. Massagué, A poised chromatin platform for TGF-β access to master regulators. *Cell* **147**, 1511–1524 (2011).
9. R. H. Xu, T. L. Sampsell-Barron, F. Gu, S. Root, R. M. Peck, G. Pan, J. Yu, J. Antosiewicz-Bourget, S. Tian, R. Stewart, J. A. Thomson, *NANOG* is a direct target of TGFβ/activin-mediated SMAD signaling in human ESCs. *Cell Stem Cell* **3**, 196–206 (2008).
10. N. Maherali, K. Hochedlinger, Tgfβ signal inhibition cooperates in the induction of iPSCs and replaces Sox2 and cMyc. *Curr. Biol.* **19**, 1718–1723 (2009).
11. J. K. Ichida, J. Blanchard, K. Lam, E. Y. Son, J. E. Chung, D. Egli, K. M. Loh, A. C. Carter, F. P. Di Giorgio, K. Koszka, D. Huangfu, H. Akutsu, D. R. Liu, L. L. Rubin, K. Eggan, A small-molecule inhibitor of tgf-β signaling replaces *Sox2* in reprogramming by inducing *Nanog*. *Cell Stem Cell* **5**, 491–503 (2009).
12. R. N. D'Souza, A. Cavender, D. Dickinson, A. Roberts, J. Letterio, TGF-β1 is essential for the homeostasis of the dentin-pulp complex. *Eur. J. Oral Sci.* **106** (Suppl. 1), 185–191 (1998).
13. A. J. Smith, N. Cassidy, H. Perry, C. Bègue-Kirn, J. V. Ruch, H. Lesot, Reactionary dentinogenesis. *Int. J. Dev. Biol.* **39**, 273–280 (1995).
14. P. D. Brown, L. M. Wakefield, A. D. Levinson, M. B. Sporn, Physicochemical activation of recombinant latent transforming growth factor-β's 1, 2, and 3. *Growth Factors* **3**, 35–43 (1990).
15. E. Mester, A. F. Mester, A. Mester, The biomedical effects of laser application. *Lasers Surg. Med.* **5**, 31–39 (1985).
16. H. Tuby, L. Maltz, U. Oron, Induction of autologous mesenchymal stem cells in the bone marrow by low-level laser therapy has profound beneficial effects on the infarcted rat heart. *Lasers Surg. Med.* **43**, 401–409 (2011).
17. B. Mvula, T. Mathope, T. Moore, H. Abrahamse, The effect of low level laser irradiation on adult human adipose derived stem cells. *Lasers Med. Sci.* **23**, 277–282 (2008).
18. J. F. Hou, H. Zhang, X. Yuan, J. Li, Y. J. Wei, S. S. Hu, In vitro effects of low-level laser irradiation for bone marrow mesenchymal stem cells: Proliferation, growth factors secretion and myogenic differentiation. *Lasers Surg. Med.* **40**, 726–733 (2008).
19. H. P. Wu, M. A. Persinger, Increased mobility and stem-cell proliferation rate in *Dugesia tigrina* induced by 880 nm light emitting diode. *J. Photochem. Photobiol. B* **102**, 156–160 (2011).
20. G. Colombo, M. Clerici, D. Giustarini, R. Rossi, A. Milzani, I. Dalle-Donne, Redox albuminomics: Oxidized albumin in human diseases. *Antioxid. Redox Signal.* **17**, 1515–1527 (2012).
21. P. R. Arany, R. S. Nayak, S. Hallikerimath, A. M. Limaye, A. D. Kale, P. Kondaiah, Activation of latent TGF-β1 by low-power laser in vitro correlates with increased TGF-β1 levels in laser-enhanced oral wound healing. *Wound Repair Regen.* **15**, 866–874 (2007).
22. K. R. Byrnes, R. W. Waynant, I. K. Ilev, X. Wu, L. Barna, K. Smith, R. Heckert, H. Gerst, J. J. Anders, Light promotes regeneration and functional recovery and alters the immune response after spinal cord injury. *Lasers Surg. Med.* **36**, 171–185 (2005).
23. M. Shi, J. Zhu, R. Wang, X. Chen, L. Mi, T. Walz, T. A. Springer, Latent TGF-β structure and activation. *Nature* **474**, 343–349 (2011).
24. J. M. Yingling, M. B. Datto, C. Wong, J. P. Frederick, N. T. Liberati, X. F. Wang, Tumor suppressor Smad4 is a transforming growth factor β-inducible DNA binding protein. *Mol. Cell. Biol.* **17**, 7019–7028 (1997).
25. M. F. Jobling, J. D. Mott, M. T. Finnegan, V. Jurukovski, A. C. Erickson, P. J. Walian, S. E. Taylor, S. Ledbetter, C. M. Lawrence, D. B. Rifkin, M. H. Barcellos-Hoff, Isoform-specific activation of latent transforming growth factor β (LTGF-β) by reactive oxygen species. *Radiat. Res.* **166**, 839–848 (2006).
26. A. J. Sloan, A. J. Smith, Stimulation of the dentine–pulp complex of rat incisor teeth by transforming growth factor-β isoforms 1–3 in vitro. *Arch. Oral Biol.* **44**, 149–156 (1999).
27. C. Bègue-Kirn, A. J. Smith, J. V. Ruch, J. M. Wozney, A. Purchio, D. Hartmann, H. Lesot, Effects of dentin proteins, transforming growth factor β1 (TGFβ1) and bone morphogenetic protein 2 (BMP2) on the differentiation of odontoblast in vitro. *Int. J. Dev. Biol.* **36**, 491–503 (1992).
28. S. Gronthos, M. Mankani, J. Brahim, P. G. Robey, S. Shi, Postnatal human dental pulp stem cells (DPSCs) in vitro and in vivo. *Proc. Natl. Acad. Sci. U.S.A.* **97**, 13625–13630 (2000).
29. I. Kobayashi, T. Kiyoshima, H. Wada, K. Matsuo, K. Nonaka, J. Y. Honda, K. Koyano, H. Sakai, Type II/III Runx2/Cbfa1 is required for tooth germ development. *Bone* **38**, 836–844 (2006).
30. S. Chen, S. Takanashi, Q. Zhang, W. Xiong, S. Zhu, E. C. Peters, S. Ding, P. G. Schultz, Reversine increases the plasticity of lineage-committed mammalian cells. *Proc. Natl. Acad. Sci. U.S.A.* **104**, 10482–10487 (2007).
31. W. T. Butler, H. Ritchie, The nature and functional significance of dentin extracellular matrix proteins. *Int. J. Dev. Biol.* **39**, 169–179 (1995).
32. J. L. Wrana, L. Attisano, J. Cárcamo, A. Zentella, J. Doody, M. Laiho, X. F. Wang, J. Massagué, TGFβ signals through a heteromeric protein kinase receptor complex. *Cell* **71**, 1003–1014 (1992).
33. P. Levéen, J. Larsson, M. Ehinger, C. M. Cilio, M. Sundler, L. J. Sjöstrand, R. Holmdahl, S. Karlsson, Induced disruption of the transforming growth factor beta type II receptor gene in mice causes a lethal inflammatory disorder that is transplantable. *Blood* **100**, 560–568 (2002).
34. N. Haruyama, T. Thyagarajan, Z. Skobe, J. T. Wright, D. Septier, T. L. Sreenath, M. Goldberg, A. B. Kulkarni, Overexpression of transforming growth factor-β1 in teeth results in detachment of ameloblasts and enamel defects. *Eur. J. Oral Sci.* **114** (Suppl. 1), 30–34 (2006).
35. L. A. Sena, N. S. Chandel, Physiological roles of mitochondrial reactive oxygen species. *Mol. Cell* **48**, 158–167 (2012).
36. S. M. Baker, R. V. Sugars, M. Wendel, A. J. Smith, R. J. Waddington, P. R. Cooper, A. J. Sloan, TGF-β/extracellular matrix interactions in dentin matrix: A role in regulating sequestration and protection of bioactivity. *Calcif. Tissue Int.* **85**, 66–74 (2009).
37. G. C. Blobe, W. P. Schiemann, H. F. Lodish, Role of transforming growth factor β in human disease. *N. Engl. J. Med.* **342**, 1350–1358 (2000).
38. P. E. Murray, A. A. Hafez, A. J. Smith, L. J. Windsor, C. F. Cox, Histomorphometric analysis of odontoblast-like cell numbers and dentine bridge secretory activity following pulp exposure. *Int. Endod. J.* **36**, 106–116 (2003).
39. T. I. Karu, L. V. Pyatibrat, S. F. Kolyakov, N. I. Afanasyeva, Absorption measurements of a cell monolayer relevant to phototherapy: Reduction of cytochrome c oxidase under near IR radiation. *J. Photochem. Photobiol. B* **81**, 98–106 (2005).
40. P. Niethammer, C. Grabher, A. T. Look, T. J. Mitchison, A tissue-scale gradient of hydrogen peroxide mediates rapid wound detection in zebrafish. *Nature* **459**, 996–999 (2009).
41. T. A. Mustoe, J. Purdy, P. Gramates, T. F. Deuel, A. Thomason, G. F. Pierce, Reversal of impaired wound healing in irradiated rats by platelet-derived growth factor-BB. *Am. J. Surg.* **158**, 345–350 (1989).
42. W. F. McKay, S. M. Peckham, J. M. Badura, A comprehensive clinical review of recombinant human bone morphogenetic protein-2 (INFUSE Bone Graft). *Int. Orthop.* **31**, 729–734 (2007).
43. S. Simon, P. Cooper, A. Smith, B. Picard, C. N. Ifi, A. Berdal, Evaluation of a new laboratory model for pulp healing: Preliminary study. *Int. Endod. J.* **41**, 781–790 (2008).

44. J. V. Ruch, H. Lesot, C. Bègue-Kirn, Odontoblast differentiation. *Int. J. Dev. Biol.* **39**, 51–68 (1995).
45. T. L. Sreenath, A. Cho, M. MacDougall, A. B. Kulkarni, Spatial and temporal activity of the dentin sialophosphoprotein gene promoter: Differential regulation in odontoblasts and ameloblasts. *Int. J. Dev. Biol.* **43**, 509–516 (1999).

Acknowledgments: We thank D. Rifkin (New York University Medical Center) for the p3TP reporter; T. Bottero (University of Michigan) for the MDPC-23 cells; W. Chou (New York University Medical Center) for the MEFs; F. Kosar (Center for Nanosciences) for μCT guidance; C. Johnson (Wyss Institute) for help with liquid chromatography–mass spectrometry; S. Karlsson (Lund University) for *TGF-βRII*$^{fl/fl}$ mice; V. Rodrigues (Harvard School of Dental Medicine) for hard tissue processing; P. Wang (Bruker Optics) for help with Raman spectroscopy; R Betensky (Harvard School of Public Health) for assistance with biostatistics; and B. Olsen, J. Garlick, and R. Maas (PRA thesis committee) for their critical, insightful suggestions. **Funding:** R37-DE-013349 (D.J.M.), R01-DE019023-01, R01-AI-050875 (M.R.H.), ZIA-DE-000698 (A.B.K.), Harvard Presidential Scholarship (P.R.A.), Wyss institute, Harvard Catalyst, Harvard Clinical and Translational Science Center [National Center for Research Resources (NCRR) and National Center for Advancing Translational Sciences (NCATS), NIH, 1UL1 TR001102-01, and financial contributions from Harvard University and its affiliated academic health care centers], and the intramural research program, NIDCR, NIH (A.B.K. and P.R.A.). The content is solely the responsibility of the authors and does not necessarily represent the official views of Harvard Catalyst, Harvard University and its affiliated academic health care centers, or the NIH. **Author contributions:** P.R.A. designed and performed experiments, analyzed data, and wrote the manuscript; T.D.H., G.S., G.X.H., K.S., E.H., J.W., and A.C.-H.C. performed biochemical and imaging experiments; A.B.K. and A.C. generated the transgenic mice; B.L.P. provided human tooth samples and helped design dental stem cell experiments; M.R.H., M.H.B.-H., and A.B.K. provided reagents, critically analyzed data, and helped write the manuscript; D.J.M. designed and analyzed experiments and wrote the manuscript. **Competing interests:** The authors declare that they have no competing interests. D.J.M. and P.R.A. are inventors on a patent application filed on this work. **Data and materials availability:** All non-commercial materials used in this study were procured via individual material transfer agreements and are acknowledged appropriately.

Submitted 11 December 2013
Accepted 10 April 2014
Published 28 May 2014
10.1126/scitranslmed.3008234

Citation: P. R. Arany, A. Cho, T. D. Hunt, G. Sidhu, K. Shin, E. Hahm, G. X. Huang, J. Weaver, A. C.-H. Chen, B. L. Padwa, M. R. Hamblin, M. H. Barcellos-Hoff, A. B. Kulkarni, D. J. Mooney, Photoactivation of endogenous latent transforming growth factor–β1 directs dental stem cell differentiation for regeneration. *Sci. Transl. Med.* **6**, 238ra69 (2014).